J Supercond Nov Magn (2011) 24: 381–390
DOI 10.1007/s10948-010-0998-z

ORIGINAL PAPER

# Influence of Diffusion-Annealing Temperature on the Physico-Mechanical Properties of Au-doped Bi-2223 Superconductors

**O. Ozturk · C. Terzioglu · I. Belenli**

Received: 10 September 2010 / Accepted: 15 September 2010 / Published online: 8 October 2010


**Abstract** In order to investigate the influence of Au doping and diffusion-annealing temperature on the mechanical and superconducting properties of Bi-2223, $Bi_{1.8}Pb_{0.35}Sr_{1.9}Ca_{2.1}Cu_3O_y$ superconductors were prepared by standard solid-state reaction methods. Doping of Bi-2223 was carried out by means of gold diffusion during sintering from an evaporated gold film on pellets. The investigation consisted of scanning electron microscopy, dc resistivity and hardness measurements. Electrical-resistivity measurements indicated that the room-temperature resistivity value decreased with decreasing diffusion-annealing temperature from 830 to 500 °C and these samples (G830, G800, G750, G700, G600 and G500) show the resistive behavior above the onset critical transition temperature with the zero-resistivity transition temperatures of 104 K, 80 K, 98 K, 95 K, 102 K and 103 K, respectively. To investigate mechanical properties of the samples, we have measured the diagonal length as a function of test load in the range of 0.245–2.940 N. Mechanical properties (microhardness, Young's modulus, yield strength and fracture toughness) of the samples are found to be load and diffusion-annealing temperature dependent. In addition, we have calculated the load independent hardness, Young's modulus, yield strength, and fracture toughness of the samples. The possible reasons for the observed changes in superconducting and mechanical properties due to Au diffusion and diffusion-annealing temperature were discussed.

O. Ozturk (✉)
Department of Physics, Faculty of Science and Arts, Kastamonu University, 37100 Kuzeykent, Kastamonu, Turkey
e-mail: oozturk@kastamonu.edu.tr

C. Terzioglu · I. Belenli
Department of Physics, Faculty of Science and Arts, Abant Izzet Baysal University, 14280 Golkoy, Bolu, Turkey

**Keywords** Mechanical properties of BSCCO · Bi-2223 · Au doping · Bi-based cuprates · Microhardness

## 1 Introduction

Engineering applications of high critical temperature ($T_c$) superconducting ceramics are generally restricted because of their brittleness. Therefore, improvement of the mechanical properties of BSCCO is a major research objective and very important for their practical applications and high performance such as quasi-permanent magnets and current leads. Hardness is a mechanical parameter and it is strongly related to the structure and composition of solids. The Vickers microhardness test is one of the convenient methods to estimate the mechanical properties. Many investigations have confirmed that the apparent (load dependent) hardness of materials is a function of the applied load. In another words, the experimentally measured hardness decreases with increasing applied load, which is called indentation size effect (ISE).

It is worth to mention that the annealing step is one of the important parts of the wire production process where one can control the physical and mechanical properties of high-$T_c$ superconductors. There are many researches about the effect of annealing time and temperature on microstructure, superconducting and mechanical properties of high-$T_c$ superconductors [1–5]. Many studies of doping into superconductor oxide ceramics have been made in order to improve their mechanical and superconducting properties [6–12]. In our previous works, we have studied the effect of the gold diffusion and diffusion-annealing time on the crystal structure, superconducting and mechanical properties of Bi-2223 samples [13, 14]. In these works, it was observed that Au

doping of the samples increased the critical transition temperature and the critical current density from $100 \pm 0.2$ K to $106 \pm 0.2$ K and from 40 to 150 A cm$^{-2}$, respectively, in comparison with those of undoped samples. It was also seen that Au doping of the samples improved the mechanical properties of the $Bi_{1.8}Pb_{0.35}Sr_{1.9}Ca_{2.1}Cu_3O_y$. We also investigated the ISE by using different models such as Meyer's law, Hay–Kendall approach and modified proportional specimen resistance model. The Hay–Kendall approach was sufficient for describing the observed ISE. In addition, diffusion of gold in $Bi_{1.8}Pb_{0.35}Sr_{1.9}Ca_{2.1}Cu_3O_y$ superconductors was investigated by means of successive removal of thin layers and measurement of the sample's resistivity at room temperature [15]. It was shown that the temperature dependence of gold diffusion at 500–830 °C is described by the relation $D = 4 \times 10^{-4} \exp(-1.08\ \text{eV}/k_B T)$.

In the present work, the effect of Au doping and diffusion-annealing temperature on the superconducting and mechanical properties of BSCCO ceramics has been investigated by performing dc electrical-resistivity measurements for electrical and superconducting properties (room-temperature resistivity, critical transition temperature and critical current density), microhardness measurements for mechanical properties (load dependent and independent of hardness, Young's modulus, yield strength, and fracture toughness), and scanning electron microscopy (SEM) for microstructure examination of the samples considered.

## 2 Experimental Details

Superconducting $Bi_{1.8}Pb_{0.35}Sr_{1.9}Ca_{2.1}Cu_3O_y$ samples were prepared by the standard solid-state reaction method [13]. Doping of Au in Bi-2223 was carried out by means of diffusion from evaporation on pellets. For diffusion-annealing temperature investigations, each gold evaporated Bi-2223 sample is annealed at 830, 800, 750, 700, 600 and 500 °C for 10 h. Typical dimensions of the samples for transport, XRD and SEM analyses were $2 \times 4 \times 10$ mm$^3$.

The resistivity as a function of temperature between 60 and 130 K was performed by a standard dc four-probe method (running a 5 mA dc current through the samples) in the cryostat. Both voltage and current contacts were made with silver paint. The transition temperature $T_c$ was defined as the zero-resistivity critical temperature in the usual sense.

The surface morphologies of the Au-diffused and pure samples were studied by using a Philips XL30 SFEG scanning electron microscope (SEM).

Hardness measurements of Au-doped Bi-2223 superconductors were performed with a digital microhardness tester (Instron Series 2100) at room temperature. A Vickers pyramidal indenter with different loads (0.245, 0.490, 0.980, 1.960, and 2.940 N) and a single loading time of 10 s were applied and the diagonals of indentation were measured with an accuracy of ±0.1 μm. Indentations were made at different parts of the samples' surface in such a way that the distance between any two indentations was no less than two times the diagonal of the indentation mark to avoid surface effects due to neighboring indentation. An average of ten readings at different locations of specimen surfaces was taken as sufficient to obtain reasonable mean values for each load.

The Vickers microhardness (load dependent) values of different applied loads were calculated by using the equation

$$H_v = 1854.4\left(F/d^2\right)\ (\text{GPa}) \tag{1}$$

where $F$ is the applied load in $N$ and $d$ is the diagonal length of the indentation mark in μm.

In most materials, the elastic modulus (Young's modulus), $E$, is related to the bulk hardness by the relation [16]

$$E = 81.9635 H_v, \tag{2}$$

and the yield strength $Y$ is related to the hardness by the relation [17, 18]

$$Y \approx H_v/3. \tag{3}$$

It is useful to mention the fracture toughness, $K_{IC}$, as it is one of the main mechanical properties of superconducting samples. The fracture toughness is an important parameter for the selection of materials for applications. Due to the nature of intrinsic brittleness, microindentation may result in microfracture around the impressed region on the surface of the samples [19]. Since microfracture occurs mainly during the loading, a portion of the energy, which is used to create the indentation deformation, will be dissipated by the crack formation. Owing to the definition of the $K_{IC}$ as the critical stress intensity factor, it is directly related to $\gamma$ (the surface energy) of the crack faces [20],

$$K_{IC} = \sqrt{2E\gamma}. \tag{4}$$

Here $E$ is Young's modulus.

## 3 Results and Discussion

### 3.1 SEM Observations

The samples of Bi-2223 tablets will be hereafter denoted as G830, G800, G750, G700, G600, G500 and P830 (gold-diffused samples annealed at 830, 800, 750, 700, 600, 500 °C and undoped sample annealed at 830 °C for 10 h, respectively). The structure of the surface morphology of the gold doped Bi(Pb)–Sr–Ca–Cu–O was studied by SEM

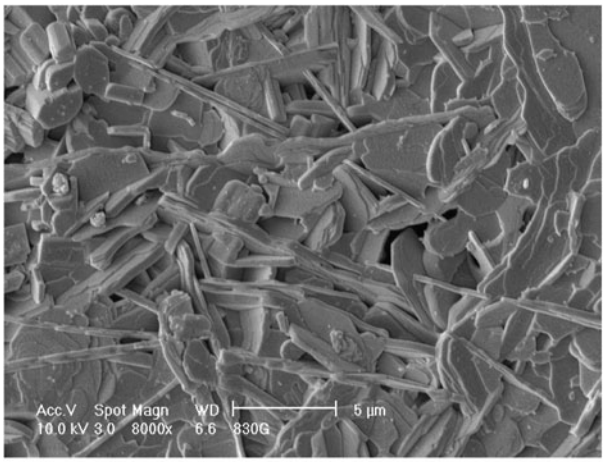


(a)

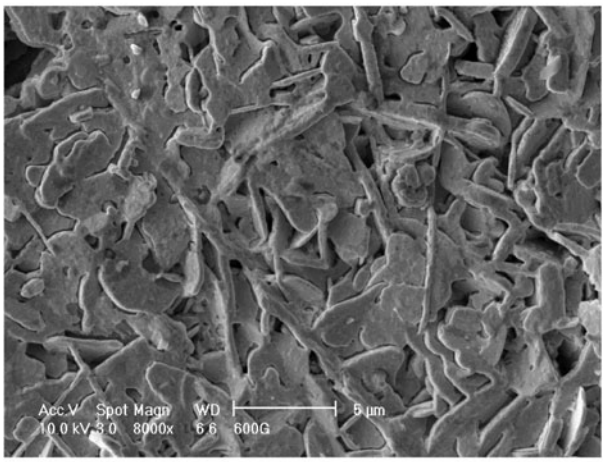


(b)

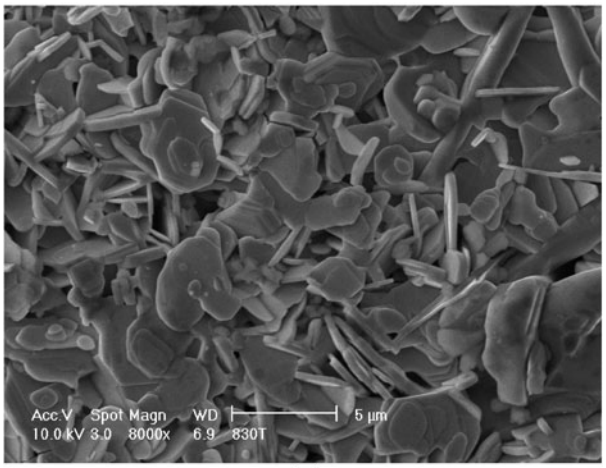


(c)

**Fig. 1** SEM micrographs of the (**a**) G830, (**b**) G600, and (**c**) P830 samples

in order to determine the grain size and possible precipitation at the grain boundaries. Figure 1 represents surface micrographs for the G830, G600 and P830 samples. The grain size of the G830 sample is relatively bigger than that of the G600 and P830 samples. The surface of the G830 sample is smoother and denser. P830 has non-uniform surface appearance with smaller grains. Moreover, the grain size of gold doped samples improved with higher diffusion-annealing temperature. SEM pictures of the surface of the samples annealed at lower temperatures present completely different morphology, indicating a metallic layer not diffused into the sample during annealing. Gold film on the sample forms a metallic connection; this resistive short-circuit connects the grains and lowers the room-temperature resistivity and improves the microhardness values of the samples as will be confirmed later on by dc resistivity and Vickers microhardness measurements, respectively. This effect continues even when gold film is diffused into the sample, indicating the gold's effect on grain boundary properties. SEM pictures show better grain connectivity in gold coated samples after heat treatment at 830 °C for 10 h.

The undoped (P830) sample consists of flake-type grains as shown in Fig. 1 and the composition of flake-type grains is approximately equal to the Bi-2212 phase [9, 21]. From the figure, one can say that the grains in the P830 sample are oriented randomly and poorly connected. The flake-like grains are less dominant in sample G830 with respect to sample P830, while the concentration of the needle-like grains grew gradually. The needle-like grains are believed to be due to the Bi-2223 phase [9, 21, 22]. These results indicate that the surface morphology of the sample is relatively improved by Au doping.

### 3.2 Electrical Measurements

In order to estimate the effect of diffusion-annealing temperature on the superconducting properties of the samples, we performed electrical-resistivity measurements. Figure 2 shows the temperature variation of the normalized (at $T =$ 130 K) resistivity of G830, G800, G750, G700, G600, G500 and P830 samples. Zero-resistivity transition temperatures of the samples are determined as 104 K, 80 K, 98 K, 95 K, 102 K, 103 K and 100 K, respectively. This pattern of the behavior is attributable to annealing temperature rather than gold doping. Annealing temperatures close to the optimum annealing temperature of 830 °C cause more degradation in superconducting properties than the lower ones. 800 °C, 750 °C and 700 °C annealing temperatures are believed to produce impurity phases through phase segregation while 600 °C and 500 °C annealing only change oxygen content of the samples. In addition to this suggestion, the existence of impurity phase in the samples annealed at relatively high temperature could be correlated with the observed double transition of resistivity in Fig. 2 for G800, G750 and G700 samples. This double transition could be related to these impurity phases which may play the role of weak links at the

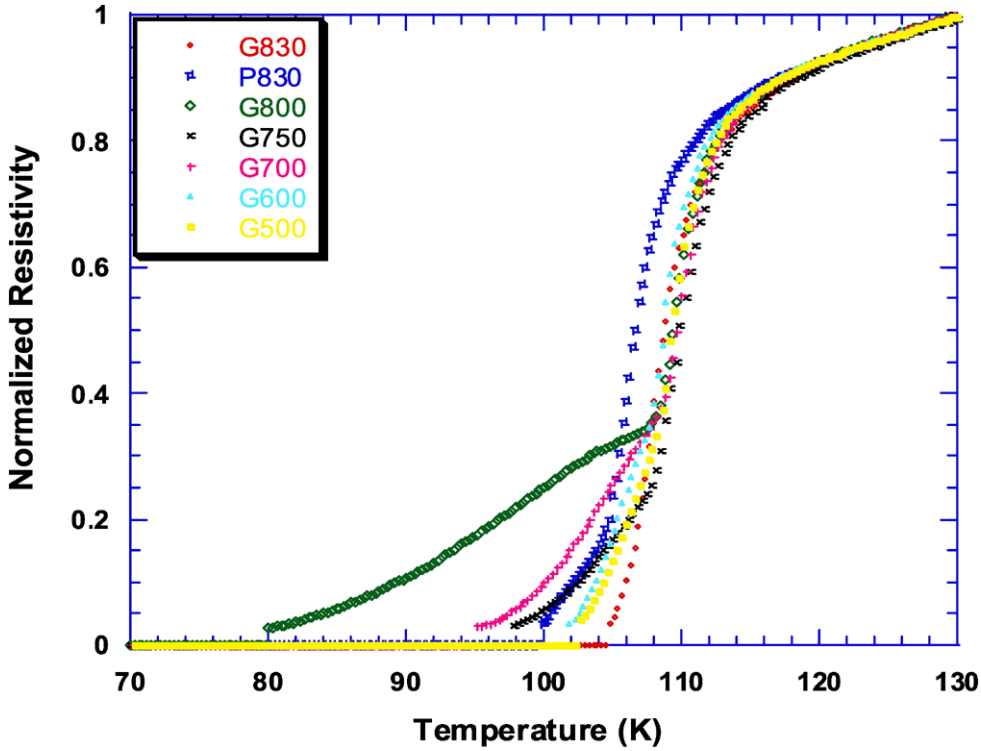


**Fig. 2** Curves of normalized resistivity as a function of temperature for the samples

**Table 1** XRD and resistivity measurements results of the samples

| Samples | Critical temperature $T_c^{offset}$ (K) | Lattice parameter $c$ (Å) | Critical current density $J_c^{trans}$ (A/cm$^2$) | Phase ratio (%) | | Room temperature resistivity $\rho$ (mΩ.cm) |
|---|---|---|---|---|---|---|
| | | | | 2212 | 2223 | |
| G830 | 104 | 37.030 | 125 | 23 | 77 | 7.10 |
| G800 | 80 | – | 4 | – | – | 5.70 |
| G750 | 98 | – | 12 | – | – | 4.80 |
| G700 | 95 | – | 8 | – | – | 4.20 |
| G600 | 102 | – | 35 | – | – | 3.50 |
| G500 | 103 | – | 38 | – | – | 3.20 |
| P830 | 100 | 36.960 | 40 | 33 | 67 | 8.50 |

grain boundaries [23]. Moreover, the critical current density ($J_c$) is affected by these weak links, so $J_c$ values decreased for G800, G750 and G700 samples, as can be seen from Table 1. The effect of gold doping is apparent in resistive tails which are shorter in a gold doped sample when compared with G830 and P830 samples. Metallic behavior is observed for all samples above the onset temperature. It is observed that the zero-resistivity transition temperature of the G830 (104 K) is higher than that for the P830 sample (100 K), this being in agreement with literature [24]. The room-temperature resistivity value of all samples decreased with decreasing diffusion-annealing temperature, as tabulated in Table 1.

In our previous work, we studied the effect of the gold diffusion and diffusion-annealing time on the crystal structure, superconducting properties of Bi-2223 samples [13]. In that work, the effect of diffusion-annealing time on microstructure and superconducting properties of Au-diffusion in Bi-2223 was investigated. It was observed that Au doping of the samples increased the critical transition temperature and the critical current density from $100 \pm 1$ K to $106 \pm 1$ K and from 40 to 150 A cm$^{-2}$, in comparison with those of undoped samples.

### 3.3 XRD Characterizations

XRD data results of samples taken from our previous work [14] are summarized in Table 1. It was obtained that the diffusion of Au increased the lattice parameter $c$ and intensity of the peaks for the Au-doped sample (G830) in comparison with that for the undoped sample (P830). This finding is in agreement with a previous work [24]. The increase

in lattice parameter $c$ revealed that cations of the system ($Bi^{+3}$, $Sr^{+2}$, $Ca^{+2}$) may partly be substituted by Au ions (0.85 Å) and the increase in the intensities of the peaks for the G830 sample may testify to the enhanced grain growth and orientation of grains with Au diffusion. The observed increase of $T_c$ makes the substitution at the Cu site less likely. As seen in the table, the volume fraction of Bi-2223 phase increased and that of Bi-2212 phase decreased with increasing Au diffusion. The diffusion gold doping of the sample improves the formation of the high-$T_c$ Bi-2223 phase in comparison with undoped sample as confirmed by the SEM micrographs.

### 3.4 Microhardness Analysis

In order to estimate the effect of Au doping and diffusion-annealing temperature on the mechanical properties of the samples, we measured the diagonal length as a function of test load. The measured indentation diagonal lengths and calculated load dependent microhardness values using (1) for different applied loads are summarized in Table 2. One can easily see that the microhardness values for all samples show a strong dependence on applied indentation loads irrespective of the Au doping and different diffusion-annealing temperature, although the numerical values are different. The values of $H_v$ at 2.94 N for G830, G800, G750, G700, G600, G500 and P830 samples are 0.270, 0.184, 0.224, 0.208, 0.245, 0.258 and 0.259 GPa, respectively. This similar change in $H_v$ with respect to the diffusion-annealing temperature is revealed for the critical transition temperature. The increased value of $H_v$ in the G830 sample compared with the P830 in our investigations can be interpreted as a result of gold diffusion in intergrain boundaries. This in turn causes the increase of intergrain contact surface or decreasing the intergrain resistivity as can be seen in Fig. 2. Figure 3 displays the changes of Vickers hardness estimated from indentations performed on sample's surfaces as a function of the applied load for the G830, G800, G750, G700, G600, G500 and P830 samples. The rapid variation of the microhardness was observed with increasing applied load from 0.245 to 1.960 N. The reason for this behavior is the contribution of weak grain boundaries [25]. It is also obvious from the figure that the Vickers microhardness values are load dependent for all samples; the calculated microhardness value decreases non-linearly as the applied load decreased until 1.960 N, then it tends to attain saturation. This non-linear behavior has also been reported in the literature for Bi–Pb–Sr–Ca–Cu–O samples [9, 10, 13] and is known as the indentation size effect (ISE) [26–29]. As reported by Kolemen et al. [30], this effect can be explained qualitatively on the basis of penetration depth of the indenter. Since indenter penetrates only surface layers at small applied loads, the surface effect is more pronounced. However, as the depth of penetration increases, the effect of the inner layers becomes more and more prominent and ultimately there is no change in the values of hardness with load.

**Table 2** The calculated load dependent $H_v$, $E$, $Y$, and $K_{IC}$ for the samples

| Sample | $F$ (N) | $d$ (μm) | $H_v$ (GPa) | $E$ (GPa) | $Y$ (GPa) | $K_{IC}$ (Pa/$\sqrt{m}$) |
|---|---|---|---|---|---|---|
| G830 | 0.245 | 29.7 | 0.515 | 42.22 | 0.172 | 545.4 |
| | 0.490 | 50.4 | 0.358 | 29.32 | 0.119 | 454.5 |
| | 0.980 | 77.6 | 0.302 | 24.74 | 0.101 | 417.5 |
| | 1.960 | 115.3 | 0.273 | 22.41 | 0.091 | 397.4 |
| | 2.940 | 142.0 | 0.270 | 22.16 | 0.090 | 395.2 |
| G800 | 0.245 | 45.0 | 0.224 | 18.36 | 0.075 | 151.5 |
| | 0.490 | 70.0 | 0.195 | 15.98 | 0.065 | 141.4 |
| | 0.980 | 98.5 | 0.187 | 15.33 | 0.062 | 138.4 |
| | 1.960 | 140.2 | 0.185 | 15.16 | 0.062 | 137.7 |
| | 2.940 | 167.0 | 0.184 | 15.08 | 0.061 | 137.3 |
| G750 | 0.245 | 37.2 | 0.328 | 26.88 | 0.109 | 208.2 |
| | 0.490 | 60.2 | 0.251 | 20.57 | 0.084 | 194.2 |
| | 0.980 | 88.3 | 0.233 | 19.10 | 0.078 | 190.2 |
| | 1.960 | 127.4 | 0.227 | 18.61 | 0.076 | 189.2 |
| | 2.940 | 155.1 | 0.224 | 18.36 | 0.075 | 188.7 |
| G700 | 0.245 | 39.3 | 0.294 | 24.09 | 0.098 | 165.3 |
| | 0.490 | 63.6 | 0.225 | 18.44 | 0.075 | 144.6 |
| | 0.980 | 91.7 | 0.216 | 17.70 | 0.072 | 139.3 |
| | 1.960 | 132.1 | 0.215 | 17.62 | 0.071 | 137.5 |
| | 2.940 | 159.1 | 0.208 | 17.05 | 0.069 | 136.6 |
| G600 | 0.245 | 33.4 | 0.407 | 33.36 | 0.136 | 337.3 |
| | 0.490 | 55.4 | 0.298 | 24.43 | 0.099 | 295.0 |
| | 0.980 | 83.1 | 0.263 | 21.56 | 0.088 | 289.0 |
| | 1.960 | 121.4 | 0.246 | 20.16 | 0.082 | 288.4 |
| | 2.940 | 149.1 | 0.245 | 20.08 | 0.081 | 283.7 |
| G500 | 0.245 | 31.2 | 0.467 | 38.28 | 0.156 | 435.3 |
| | 0.490 | 53.0 | 0.324 | 26.56 | 0.108 | 372.5 |
| | 0.980 | 80.0 | 0.284 | 23.28 | 0.095 | 349.9 |
| | 1.960 | 117.8 | 0.262 | 21.47 | 0.087 | 338.4 |
| | 2.940 | 145.3 | 0.258 | 21.15 | 0.086 | 337.7 |
| P830 | 0.245 | 31.5 | 0.458 | 37.53 | 0.153 | 490.9 |
| | 0.490 | 53.5 | 0.317 | 26.02 | 0.106 | 408.8 |
| | 0.980 | 83.3 | 0.262 | 21.47 | 0.087 | 371.3 |
| | 1.960 | 122.1 | 0.244 | 19.98 | 0.811 | 358.2 |
| | 2.940 | 151.0 | 0.239 | 19.60 | 0.079 | 354.8 |

The values of load dependent $E$, $Y$ and $K_{IC}$ were calculated for each load by using (2)–(4), and they are summarized in Table 2. As seen in this table, the load dependent $E$, $Y$ and $K_{IC}$ increase with decreasing loads. This behavior is due to crack initiation of microhardness. A change in $E$, $Y$

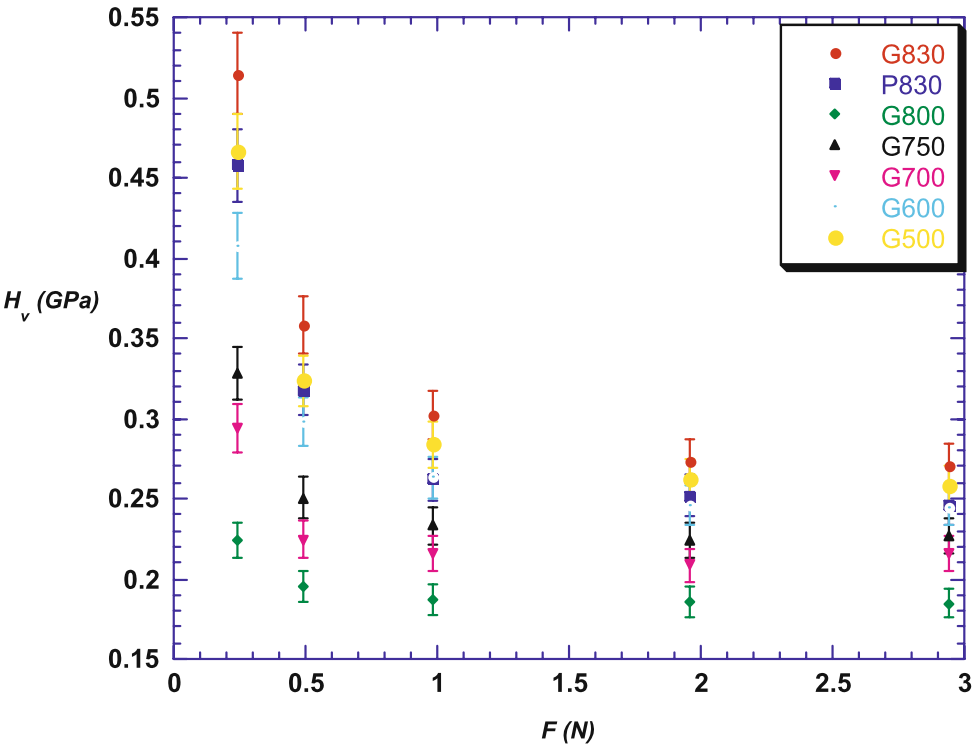


**Fig. 3** The variation of microhardness with load for the samples

and $K_{IC}$ corresponds to a change in the average surface energy as proposed from the hardness calculations. One should point out that the apparent (load dependent) microhardness, Young's modulus, yield strength and fracture toughness of the samples in the present work indicate a strong dependency on applied load.

To account for the load dependence of hardness, several relationships between the applied load and the resulting indentation size have been suggested [31–34]. This effect can be explained by two different models [35]. The first model assumes that the indentation contains an elastic portion. The elastic part of the deformation is relaxed upon loading. This can be accounted for by adding an elastic component, $d_e$, to the measured plastic indentation semidiagonal, $d_p$. Thus, a true hardness, $H_0$, is defined from [35, 36] by

$$H_0 = 1854.4\left(\frac{F}{(d_p + d_e)^2}\right) \text{ (GPa)}. \tag{5}$$

One can see from the equation that measured indentation diagonals are linear with the square root of the applied load. Figure 4 indicates $d_p$ versus $F^{1/2}$ plots for G830, G750, and P830 samples. The slope of such a curve is proportional to $(H_0)^{-1/2}$ and that of the vertical intercept is proportional to the elastic part of the indentation semi diagonal, $d_e$. The extracted values of $H_0$ and $d_e$ and the linear regression coefficients (*LRC)* for all samples are summarized in Table 3. It was obvious that such plots are linear with the estimated *LRC*, always better than 99.8%, implying that (5) provides a satisfactory description to calculate the true hardness of the indentation data for the samples. As can be seen from the table, the value of $H_0$ varies slightly but that of $d_e$ varies significantly with changing the diffusion-annealing temperature. The variation of Vickers microhardness as a function of indentation load for a variety of ceramic materials was investigated by J.B. Quinn and G.D. Quinn [37]. They observed that such a hardness-load curve shows a distinct transition to a plateau of the constant hardness level and concluded that the transition in such curves corresponds to the intrinsic hardness value of the material. In this study, this plateau is reached at 1.960 N applied load for the samples. True microhardness value of G830 sample (0.201 GPa) is lower than the saturated microhardness value (see Table 2) in the plateau region ($H_v = 0.273$ and 0.270 GPa). This behavior is observed in other samples (P830, G800, G750, G700, G600 and G500) in this work. This result indicates that the true hardness of the sample is lower than that of the traditionally calculated ones. The calculations of $H_0$ values for the investigated samples also indicated that the magnitude of $d_e$ to be 15 for P830, 2–18 μm for Au-doped samples (G830, G800, G750, G700, G600 and G500). From these extracted magnitudes of $d_e$ one infers that the amount of relaxation of diagonal length is significant with respect to the measured diagonals at low indentation loads [38] and hence the ISE is pronounced for the low load range. This method has been applied to YBaCuO and BiPbSrCaCuO [35, 38–40] materials but consistency was not very good. Although the experimental data of Fig. 4 fit well with the theoretical curve, the extracted value of $H_0$ for G830 is lower than that

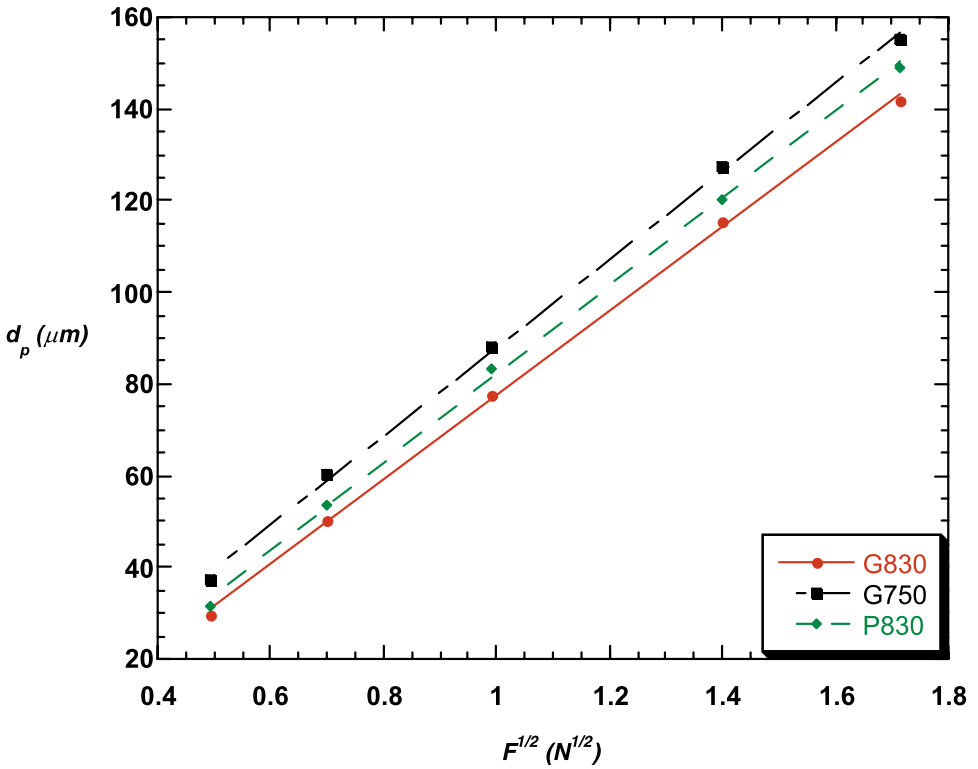


**Fig. 4** Plots of diagonal length versus square root of applied loads for the samples

**Table 3** Best-fit results of experimental data according to (5)

| Samples | $H_0$ (GPa) | $d_e$ (μm ) | *LRC* | $H_v$ (GPa) in plateau region |
|---|---|---|---|---|
| G830 | 0.201 | 18.29 | 0.99982 | 0.270–0.273 |
| G800 | 0.186 | 1.55 | 0.99883 | 0.185–0.186 |
| G750 | 0.200 | 8.34 | 0.99840 | 0.224–0.227 |
| G700 | 0.194 | 6.49 | 0.99803 | 0.208–0.215 |
| G600 | 0.207 | 11.78 | 0.99860 | 0.235–0.237 |
| G500 | 0.214 | 13.21 | 0.99961 | 0.258–0.263 |
| P830 | 0.200 | 15.30 | 0.99935 | 0.239–0.243 |

of G600 and G500. Thus, this model is not consistent for our data.

The second method considers energy dissipative processes during the indentation rather than elastic processes. In this model, a true microhardness can be defined by subtracting a dissipative part, $F_0$, from the applied load [35]:

$$H_0 = 1854.4\left(\frac{F - F_0}{d^2}\right) \text{(GPa)}. \tag{6}$$

Figure 5 shows $F$ versus $d^2$ plots for the G830, G700 and P830 samples. Each graph shows an excellent linear relationship ($LRC \succ 0.9994$). The slope of each line corresponds to the load independent hardness constant, $H_0$ and the vertical intercept of each line represents the sample resistance pressure, $F_0$. The extracted values of $F_0$, $H_0$ and *LRC* are listed in Table 4. It is observed that this similar change in $F_0$ and $H_0$ with respect to the diffusion-annealing temperature is revealed for the critical transition temperature and the load dependent microhardness values. The *LRC* of each sample is very high, implying that (6) provides a satisfactory description of the indentation data for the samples.

On the other hand, it is observed that the diagonal length is strongly dependent on the applied load from the experimental observations. This observation is governed by

$$\frac{F}{d} = H_0 d + \gamma \tag{7}$$

proposed in [13, 30, 31, 39]. Figure 6 exhibits the values of $F/d$ against the diagonal length of indentation, $d$, for the G830, G600 and P830 samples. Each set of data shows an excellent linear relationship in a narrower range of applied loads. The slope of each line corresponds to the true hardness, $H_0$, and the intercept of each line represents the surface energy, $\gamma$. The extracted values of $H_0$, $\gamma$ and *LRC* for all samples are listed in Table 5. It is observed that the value of $H_0$ varies slightly while that of $\gamma$ varies significantly with changing the diffusion-annealing temperature. This observation is ascribed to the dissipation of the energy of cracks at the interfaces [35].

In addition, we focused on load independent values of Young's modulus, yield strength, and fracture toughness of the samples. We have calculated $E$, $Y$, and $K_{IC}$ using the

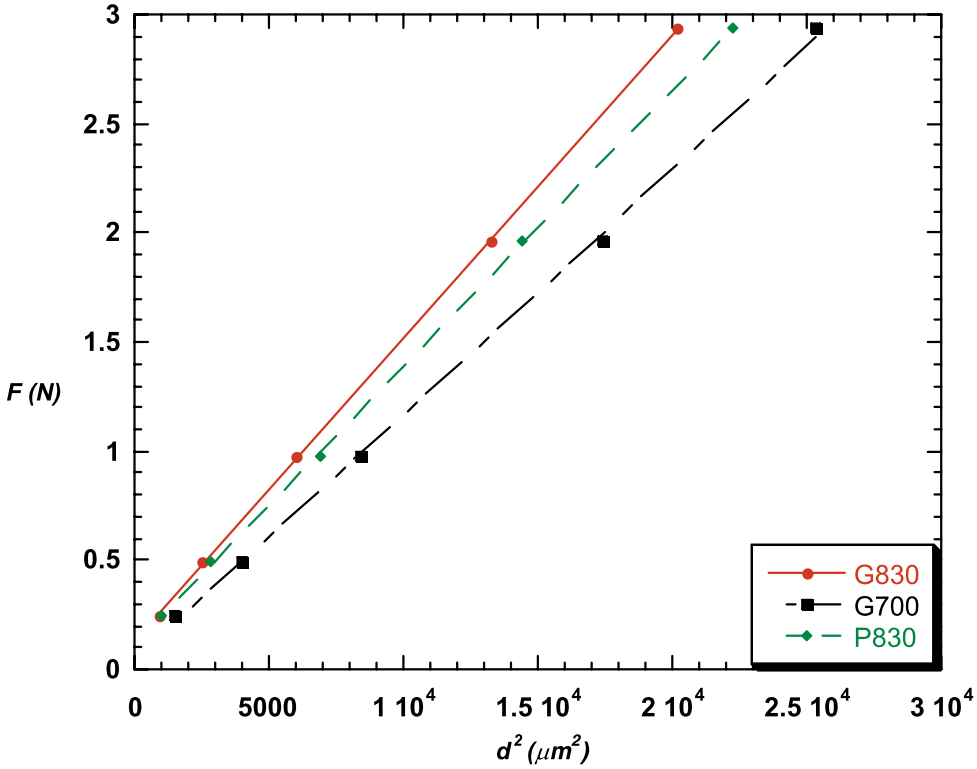


**Fig. 5** Graph of the applied load against the square of the diagonal length for the samples

**Table 4** Best-fit results of experimental data according to (6)

| Samples | $H_0$ (GPa) | $F_0$ (N) | *LRC* |
|---|---|---|---|
| G830 | 0.138 | 0.131 | 0.99998 |
| G800 | 0.104 | 0.009 | 0.99986 |
| G750 | 0.119 | 0.062 | 0.99983 |
| G700 | 0.113 | 0.040 | 0.99946 |
| G600 | 0.127 | 0.100 | 0.99946 |
| G500 | 0.134 | 0.116 | 0.99980 |
| P830 | 0.123 | 0.128 | 0.99998 |

true microhardness (load independent, $H_0$) for each sample. The calculated load independent $Y$, $E$, and $K_{IC}$ by using (2)–(4) for each sample are tabulated in Table 6. From the table, it is observed that the load independent values of $E$, $Y$, $K_{IC}$ increase with decreasing applied loads. Comparing Tables 2 and 6, one can conclude that the load independent values are lower than that of load dependent values. This is in agreement with what is reported in the literature [35, 41]. The above results revealed that by increasing the diffusion-annealing temperature, it is possible to control the mechanical properties of the samples.

## 4 Conclusion

A microindentation method can be used to measure mechanical properties of polycrystalline superconductors such as hardness, Young's modulus, yield strength and fracture toughness. When Au-doped samples of $Bi_{1.8}Pb_{0.35}Sr_{1.9}Ca_{2.1}Cu_3O_y$ phase, prepared by solid-state reaction methods, are compared with samples annealed at different diffusion-annealing temperatures, the following statements are concluded to for doped samples:

- Resistive behavior was observed for all samples above the onset temperature.
- The room-temperature resistivity value decreased with decreasing diffusion-annealing temperature.
- Zero-resistivity transition temperatures of the samples were determined as 104 K, 80 K, 98 K, 95 K, 102 K, 103 K and 100 K for G830, G800, G750, G700, G600, G500, and P830 samples, respectively.
- The improvement of superconducting and mechanical properties is due to the modification of grain boundaries by gold doping.
- Vickers microhardness, Young's modulus, yield strength and fracture toughness values of the samples were load dependent. Their variation with load is non-linear.
- The load dependency of the hardness, Young's modulus, yield strength and fracture toughness exhibit a typical ISE.
- The ISE is examined by (5) and (6). Equation (6) is found to be more suitable for describing the experimental data.
- The load dependent values of $H_v$, $E$, $Y$, and $K_{IC}$ are greater than those of load independent values.

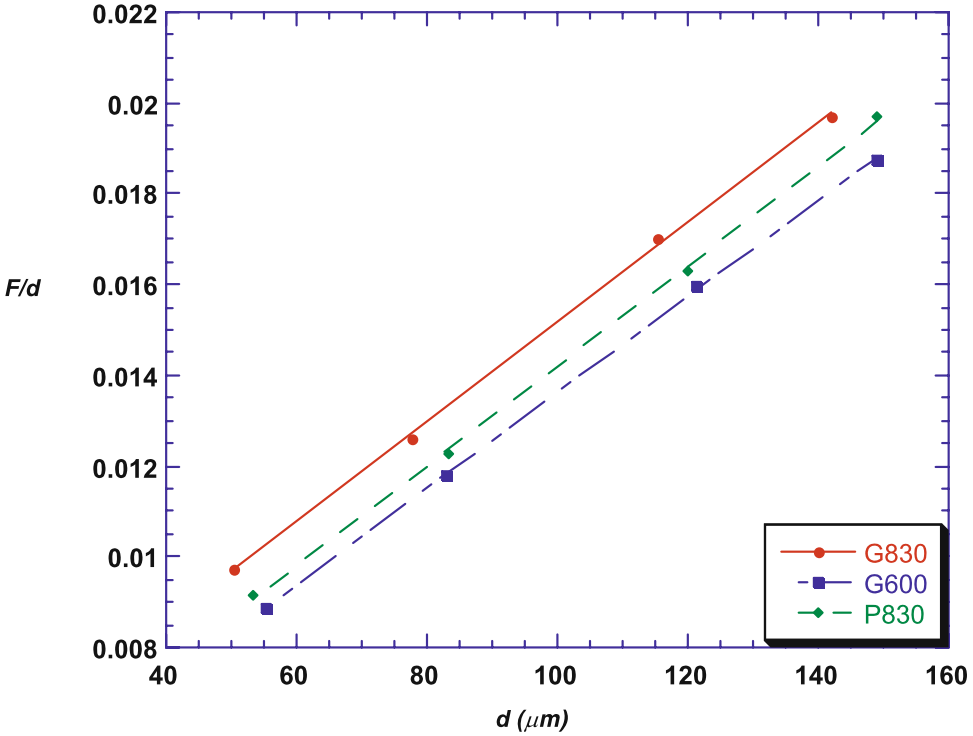


**Fig. 6** Plots of $F/d$ versus $d$ for the samples

**Table 5** Best-fit results of experimental data according to (7)

| Samples | $H_0$ (GPa) | $\gamma \times 10^{-3}$ (N/μm) | *LRC* |
|---|---|---|---|
| G830 | 0.119 | 3.523 | 0.9990 |
| G800 | 0.107 | 0.625 | 0.9991 |
| G750 | 0.113 | 1.181 | 0.9990 |
| G700 | 0.111 | 0.508 | 0.9992 |
| G600 | 0.115 | 2.360 | 0.9991 |
| G500 | 0.117 | 2.840 | 0.9990 |
| P830 | 0.106 | 3.211 | 0.9990 |

**Table 6** The calculated load independent $H_0$, $E$, $Y$, $K_{IC}$ and $B_i$ for each sample

| Samples | $H_0$ (GPa) | $E$ (GPa) | $Y$ (GPa) | $K_{IC}$ (Pa/m$^{1/2}$) |
|---|---|---|---|---|
| G830 | 0.119 | 9.754 | 0.040 | 262.2 |
| G800 | 0.107 | 8.770 | 0.036 | 104.7 |
| G750 | 0.113 | 9.262 | 0.038 | 147.9 |
| G700 | 0.111 | 9.098 | 0.037 | 96.1 |
| G600 | 0.115 | 9.426 | 0.038 | 210.9 |
| G500 | 0.117 | 9.590 | 0.039 | 233.4 |
| P830 | 0.106 | 8.689 | 0.035 | 236.2 |

- The decrease in $H_v$ is attributed to the formation of impurity phases and irregularities mainly distributed at the grain boundaries. These cause distortion of the bond strength, and consequently the hardness values decrease.

**Acknowledgement** This work is supported partly by The Scientific and Technological Council of Turkey (Project No.: 104T325) and partly by the Turkish State Planning Organization (DPT) (Project No.: 2004K120200).

## References

1. Khalil, S.M., Sedky, A.: Physica B **357**, 299 (2005)
2. Ibrahim, M.M., Khalil, S.M.: Eur. Phys. J. AP **14**, 79 (2001)
3. Sarkar, A.K., Maartense, I.: Physica C **168**, 591 (1990)
4. Khalil, S.M.: Phys. Status Solidi (a) **178**, 731 (2000)
5. Shi, L., Dong, Q., Zhang, Y.: Physica C **649**, 341–348 (2000)
6. Biju, A., Abhilash Kumar, R.G., Aloysius, R.P., Syamaprasad, U.: Physica C **449**, 109 (2006)
7. Yilmazlar, M., Cetinkara, H.A., Nursoy, M., Ozturk, O., Terzioglu, C.: Physica C **442**, 101 (2006)
8. Khalil, S.M.: Smart Mater. Struct. **14**, 804 (2005)
9. Khalil, S.M.: J. Phys. Chem. Solids **62**, 457 (2001)
10. Murakami, A., Katagiri, K., Noto, K., Kasaba, K., Sohoji, Y., Muralidhar, M., Sakai, N., Murakami, M.: Physica C **794**, 378–381 (2002)
11. Katagiri, K., Murakami, A., Kan, R., Kasaba, K., Noto, K., Muralidhar, M., Sakai, N., Murakami, M.: Physica C **526**, 392–396 (2003)
12. Terzioglu, C., Yilmazlar, M., Ozturk, O., Yanmaz, E.: Physica C **423**, 119 (2005)
13. Yilmazlar, M., Ozturk, O., Gorur, O., Belenli, I., Terzioglu, C.: Supercond. Sci. Technol. **20**, 365 (2007)
14. Nursoy, M., Yılmazlar, M., Terzioglu, C., Belenli, I.: J. Alloys Compd. **459**, 399 (2008)
15. Terzioglu, C., Ozturk, O., Belenli, I.: J. Alloys Compd. **471**, 142 (2009)

16. Veerender, C., Dumke, V.R., Nagabhooshanam, M.: Phys. Status Solidi (a) **144**, 199 (1994)
17. McClintock, F.A., Argon, A.S.: Mechanical Behaviour of Materials. Addison-Wesley, Reading (1996), p. 455
18. Tabor, D.: The Hardness of Metals. Clarendon, Oxford (1951)
19. Lawn, B.R., Wilshaw, T.R.: J. Mater. Sci. **10**, 1049 (1975)
20. Davidge, R.W.: Mechanical Behavior of Ceramics. Cambridge University Press, Cambridge (1979), pp. 31–50
21. Chen, Y.C., Chong, K.K., Meen, T.H.: Jpn. J. Appl. Phys. **30**, L33 (1991)
22. Yoon, K.H., Lee, Y.B.: J. Mater. Sci. **26**, 5101 (1991)
23. Kameli, P., Salamati, H., Eslami, M.: Solid State Commun. **137**, 30–35 (2006)
24. Dzhafarov, T.D., Altunbaş, M., Varilci, A., Küçükömeroğlu, T., Nezir, S.: Solid State Commun. **99**, 839 (1996)
25. Ling, H.C., Yan, M.F.: J. Appl. Phys. **64**, 1307 (1988)
26. Gong, J., Wu, J., Guan, Z.: Mater. Lett. **38**, 197 (1999)
27. Sangwal, K., Surowska, B.: Mater. Res. Innov. **7**, 91 (2003)
28. Tickoo, R., Tandon, R.P., Bamzai, K.K., Kotru, P.N.: Mater. Chem. Phys. **42**, 446 (2003)
29. Elmustafa, A.A., Stone, D.S.: J. Mech. Phys. Solids **51**, 357 (2003)
30. Kölemen, U., Uzun, O., Yılmazlar, M., Güçlü, N., Yanmaz, E.: J. Alloys Compd. **415**, 300 (2006)
31. Fröhlinch, F., Grau, P., Grellmann, W.: Phys. Status Solidi (a) **42**, 79 (1997)
32. Li, H., Bradt, R.C.: J. Mater. Sci. **22**, 917 (1993)
33. Hays, C., Kendall, E.G.: Metallography **6**(4), 275 (1973)
34. Gong, J., Wu, J., Guan, Z.: J. Eur. Ceram. Soc. **19**, 2625 (1999)
35. Leenders, A., Ullrich, M., Freyhardt, H.C.: Physica C **279**, 173 (1997)
36. Li, Z., Ghosh, A., Kobayashi, A.S.: J. Am. Ceram. Soc. **72**, 904 (1989)
37. Quinn, J.B., Quinn, G.D.: J. Mater. Sci. **32**, 4331 (1997)
38. Dutta, A.K., Narasaiah, N., Chattopadhyaya, A.B., Ray, K.K.: Ceram. Int. **27**, 407 (2001)
39. Hirao, K., Tomozawa, M.: J. Am. Ceram. Soc. **70**, 497 (1997)
40. Bernhardt, E.O.: Z. Metall. **33**, 135 (1941)
41. Uzun, O., Kolemen, U., Celebi, S., Guclu, N.: J. Eur. Ceram. Soc. **25**, 969 (2005)